

12-2022

## Numerical Simulation of Vibration - Based Piezoelectric Energy Harvester for Shape Comparison

Adriana Rosas  
*The University of Texas Rio Grande Valley*

Follow this and additional works at: <https://scholarworks.utrgv.edu/etd>



Part of the [Civil and Environmental Engineering Commons](#)

---

### Recommended Citation

Rosas, Adriana, "Numerical Simulation of Vibration - Based Piezoelectric Energy Harvester for Shape Comparison" (2022). *Theses and Dissertations*. 1180.  
<https://scholarworks.utrgv.edu/etd/1180>

This Thesis is brought to you for free and open access by ScholarWorks @ UTRGV. It has been accepted for inclusion in Theses and Dissertations by an authorized administrator of ScholarWorks @ UTRGV. For more information, please contact [justin.white@utrgv.edu](mailto:justin.white@utrgv.edu), [william.flores01@utrgv.edu](mailto:william.flores01@utrgv.edu).

NUMERICAL SIMULATION OF VIBRATION - BASED PIEZOELECTRIC ENERGY  
HARVESTER FOR SHAPE COMPARISON

A Thesis

by

ADRIANA ROSAS

Submitted in Partial Fulfillment of the  
Requirements for the Degree of  
MASTER OF SCIENCE

Major Subject: Civil Engineering

The University of Texas Rio Grande Valley

December 2022



NUMERICAL SIMULATION OF VIBRATION - BASED PIEZOELECTRIC ENERGY  
HARVESTER FOR SHAPE COMPARISON

A Thesis

by

ADRIANA ROSAS

COMMITTEE MEMBERS

Dr. Mohsen Amjadian  
Chair of Committee

Dr. Yooseob Song  
Committee Member

Dr. Philip Park  
Committee Member

Dr. Thang Pham  
Committee Member

December 2022



Copyright 2022 Adriana Rosas  
All Rights Reserved



## ABSTRACT

Rosas, Adriana, Numerical Simulation of Vibration - Based Piezoelectric Energy Harvester for Shape Comparison. Master of Science (MS), December, 2022, 42 pp., 3 tables, 19 figures, references, 68 titles.

This work investigates the shape optimization of piezoelectric energy harvesters subjected to mechanical vibration using ABAQUS/Standard software. Three piezoelectric energy harvesters with different dimensions but the same areas were created to identify if model dimensions have an impact on the output voltage. The models were tested at different speeds to create an output voltage. Once the output voltages were obtained, the results were compared with each other to find if shape optimization on piezoelectric energy harvesters has an impact on scavenging energy from mechanical vibrations.



DEDICATION

Para Mama y Papa



## TABLE OF CONTENTS

	Page
ABSTRACT.....	iii
DEDICATION.....	iv
TABLE OF CONTENTS.....	v
LIST OF TABLES.....	vi
LIST OF FIGURES.....	vii
CHAPTER I. INTRODUCTION.....	1
1.1 Problem Statement.....	1
1.2 Research Objective.....	3
1.3 Method and Scope of Work.....	3
CHAPTER II. LITERATURE REVIEW FOR PIEZOELECTRIC ENERGY HARVESTING.....	5
2.1 Introduction.....	5
2.2 Background.....	5
2.3 Piezoelectric Materials.....	8
2.4 Principles of Piezoelectric Effects.....	12
2.5 Shape Optimization of Piezoelectric Energy Harvesting.....	17
CHAPTER III. METHODOLOGY.....	21
3.1 Finite Element Analysis.....	21
3.2 Finite Element Modeling.....	23
3.3 Model Validation.....	27
CHAPTER IV. RESULTS.....	30
CHAPTER V. ANALYSIS.....	34
CHAPTER VI. CONCLUSION.....	35
REFERENCES.....	36
BIOGRAPHICAL SKETCH.....	42



## LIST OF TABLES

	Page
Table 1: Dimensions of PEHs .....	25
Table 2: Material Properties for the PEHs .....	25
Table 3: First and second modes of natural frequencies for theoretical validation (Song, 2019) ...	28



## LIST OF FIGURES

	Page
Figure 1: Direct Piezoelectric Effect: <b>a</b> ) at applied compressive stress <b>b</b> ) at applied tension (Dineva, Gross, Müller, & Rangelov, 2014) .....	7
Figure 2: Inverse piezoelectric effect at applied electric field (Dineva et al., 2014) .....	7
Figure 3: Natural Piezoelectric materials (Manbachi & Cobbold, 2011) .....	9
Figure 4: The seven groups of crystals (KHI, 2007) .....	10
Figure 5: Dipole of Piezoelectric effect in Quartz (Susie Maestre, 2022) .....	11
Figure 6: Direct Piezoelectric Effect. Opposite faces with a different charge due to compression of the material (Susie Maestre, 2022) .....	11
Figure 7: Electromechanical coupling of piezoelectric effect (Song, 2019).....	13
Figure 8: Axis for constitutive equation sample (Moheimani & Fleming, 2006) .....	14
Figure 9: Energy harvester geometry and dimensions (Song, 2019) .....	23
Figure 10: Top view of model L1-R3 .....	23
Figure 11: Top view of model L3-R1 .....	24
Figure 12: Top view of model REC .....	24
Figure 13: Boundary Conditions for the structure .....	26
Figure 14: Boundary conditions applied to the structure .....	27
Figure 15: Model validation from (Song, 2019).....	28
Figure 16: Schematic for the points where the vertical acceleration was obtained (Song, 2019).....	29
Figure 17: RMS results at different speeds .....	30
Figure 18: Output Voltage from the PEHs .....	31
Figure 19: REC model comparison .....	33



## CHAPTER I

### INTRODUCTION

A piezoelectric energy harvester (PEH) is a self-power source for wireless sensor network system. The piezoelectric material is known for converting mechanical vibration into electrical energy; this material can cease the increment of fossil fuels by producing renewable and clean energy from mechanical vibrations. PEHs can be embedded on pavement, harness mechanical vibration from vehicles, and convert it into energy. This energy harvesting technique can use the wasted energy from vehicles and use that same energy to power a structure health monitor, light poles, or electric snow-melting machines embedded in the pavement. Even though PEHs depend on external physical movement to create energy, the design of the PEH is essential to harness the most energy possible. The shape, area, length, thickness, and width can vary the energy harvested from a PEH.

#### **1.1 Problem Statement**

Up to the present moment, the most used energy source is fossil fuels (BP, 2021). Since pavement represents most of the transportation section, some energy-harvesting technologies like solar energy systems are already integrated into the pavement to extract energy, but this system's drawback is its dependency on weather conditions (Guldentops, Nejad, Vuye, & Rahbar, 2016; Zhou, Z. et al., 2015). According to the report Key World Energy Statics 2015 conducted by

International Energy Agency in 2013, transportation shared 63.8% of the world's oil consumption (Xiong & Wang, 2016). With the continuous growing demand in the automobile industry and the significant changes in the transportation highway system, the available vibration energy has increased (Cho et al., 2019; Lee & Choi, 2014; Tan, Zhong, Lv, Ouyang, & Zhou, 2013; Wang, C. H., Wang, & Li, 2016). According to a simulation done by (Delorme, Karbowski, & Sharer, 2010), about 11-19% of the energy gained from burning gasoline is lost on tires/rolling resistance when a class 8 truck travels at a speed of 105 km/h with 10-100% of its maximum loading. When a vehicle travels on pavement, it leaves a transformation; this is because some of its power supplied by burning gasoline is transformed into deformation and vibration. A record of the Highway Statistics 2012 prepared by the Federal Highway Administration, there are 253,639,386 registered vehicles in the United States; according to FHA, the average distance traveled by a single vehicle is 18,728 km, and 2514 L of fuel consumption per vehicle (Highway statistics 2012. federal highway administration.). Assuming that the average energy loss of a vehicle on tires is 15% (Delorme et al., 2010) and that the equivalent of energy of one liter of petrol gasoline is  $3.478 \times 10^7$  J; the total energy wasted annually by a vehicle in the United States on tires is about

$$3.478 \times 10^7 \text{ J/L} \times 2514 \text{ L} \times 253,639,386 \times 15\% \approx 2.218 \times 10^{16} \text{ kJ}$$

Implementing new technology on roads to harvest this part of the energy will benefit the current energy harvesting ecosystem. If only 1/1000 of this energy lost on roads could be captured, it would be enough to supply about 6 million houses in the United States (Xiong & Wang, 2016). There is a study of conductive asphalt and piezoelectric material layers where its power-generation characteristics were verified. According to this study, an output voltage of 7.2 V was generated with a piezoelectric module used in actual roads (Guo & Lu, 2017a). In another

study, where road energy collection was also used, a traffic signal indicator lamp was constructed based on a piezoelectric module (Najini & Muthukumaraswamy, 2016). As well as piezoelectric modules that have helped with energy-harvesting, asphalt pavement technologies have been used recently to convert vibrational energy from roads (Moure et al., 2016; Wang, Chaohui, Zhao, Li, & Li, 2018; Zhang et al., 2016). This research aims to create an optimal PEH shape capable of absorbing vibrational energy.

## **1.2 Research Objective**

To create more sustainable and clean energy sources in the future, more advanced technologies such as PEH need to be created. The energy harnessed by PEH from vehicle vibrations is an alternative to decrease the current environmental problem of harmful chemicals. This technology is already in use and has been proven to work. This research aims to analyze and study previous research about PEHs model data to design an optimal shape capable of collecting significant amounts of energy from vehicle vibrations. The results from this study should help with the understanding of how PEH works and the benefits these energy harvesters (EH) are for the environment.

## **1.3 Method and Scope of Work**

This paper utilizes ABAQUS/Standard software to create an optimal design for the PEHs. ABAQUS/Standard is a flexible tool for finite element modeling (FEM). This software is used to model and analyze mechanical components and assemblies; also, it visualizes the FE analysis.

ABAQUS has a series of steps that need to be followed to create a model. The software allows changing the procedure choice to be analyzed from step to step. Since the state of the model is updated throughout all analysis steps, the effects of previous history are always included in the response in each new step (ABAQUS Online Documentation, 2006). Allowing to change the procedure choice from step to step makes this software a flexible tool to model and analyze.

This paper includes a literature review on the origins of PEH, piezoelectric materials, piezoelectric effect principles, and PEH's shape optimization. Also, an explanation of FEM and some PEH models created in ABAQUS is presented. This study focuses on the performance of PEHs under different design factors at different velocities.

## CHAPTER II

### LITERATURE REVIEW FOR PIEZOELECTRIC ENERGY HARVESTING

#### **2.1 Introduction**

This chapter covers piezoelectric history, materials, its properties, and shape optimization on PEH throughout the years. It will begin with a brief overview of the most important events in piezoelectricity throughout its history; like the discovery of the piezoelectric effect, the process on how to create piezoelectric ceramics, its constitutive equations, and its advancements in how the shape of PEHs have changed throughout the years with the aimed to design a shape capable of absorbing the most energy possible.

Even though piezoelectricity is a well-known subject in today's professional community, it was not pervasive back in 1880. The piezoelectric effect has a tremendous impact on today's society to the point that almost if not every person in the world possesses a piezoelectric device. One of the most used and well-known devices is wristwatches; all wristwatches and clocks that have quartz as a material are based on piezoelectricity. Also, some of the most common devices that employ the piezoelectric effect are transducers, sensors, pumps, and motors.

#### **2.2 Background**

Piezoelectricity comes from Greek; the word "piezo" is defined as "to press" or "pressure". Therefore, combined with the word "electricity", it means electricity generated from

pressure. The discovery of the piezoelectric effect was reported to the French Academy of Science on August 2, 1880, by the brothers Jacques and Pierre Curie (Arnau & Soares, ; Duck, Francis, 2009; Katzir, 2006). The Curie brothers discovered that if they compressed asymmetric crystals along their hemihedral (semi-symmetric) axes, positive and negative charges would appear on opposite faces of the crystal and disappear when the pressure ceases. Some of the crystals the Curie brothers assigned at that time as materials capable of displaying surfaces charged when mechanically stressed were quartz, cane sugar, topaz, Rochelle salt, and tourmaline.

The direct piezoelectric effect was credited to the Curie brothers, Figure 1. However, they did not discover the converse piezoelectric effect. It was not until 1881 that mathematician Gabriel Lippmann demonstrated that a converse piezoelectricity effect should exist. According to Lippmann, applying an electric field to a crystal should cause a material deformation based on the fundamental laws of thermodynamics (Uchino, 2017). The new theory proposed by Lippmann caught the Curie brothers' attention; the brothers tested Lippmann's theory and confirmed that the theory about the converse effect was correct, Figure 2. Also, the Curie brothers devised the piezoelectric quartz electrometer; this device was capable of measuring faint electric currents. Pierre and Marie Curie then used this device to measure radioactivity by radium (Duck, F. A. & Thomas, 2022).

Even though the piezoelectric effect was a significant advancement in science, it went unnoticed for several decades. It was until World War I, 1914, when the piezoelectricity effect was considered a credible scientific activity (Moheimani & Fleming, 2006). Due to the catastrophic events at that time, a real investment to accelerate ultrasonic technology was made to find German U-boats underwater. In February 1917, Dr. Paul Langevin thought that maybe

quartz's piezoelectric properties could be successfully exploited initially to receive and transmit ultrasound, and after some experiments, it was concluded that his theory was correct (Duck & Thomas, 2022). The discovery was implemented to build an ultrasonic submarine detector; piezoelectric quartz crystals were subjected to alternating voltage to make the sonar transmitter vibrate; the vibration of the sonar could send ultrasound waves through the water and measure the time it took these waves to bounce back from an object and revealed how far away it was.

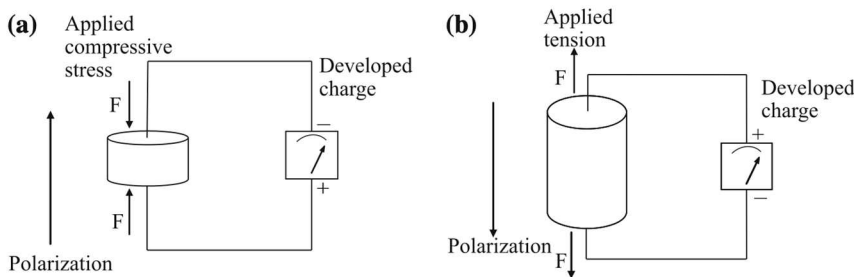


*Fig 1. Direct Piezoelectric Effect: (a) at applied compressive stress (b) at applied tension (Dineva et al., 2014)*

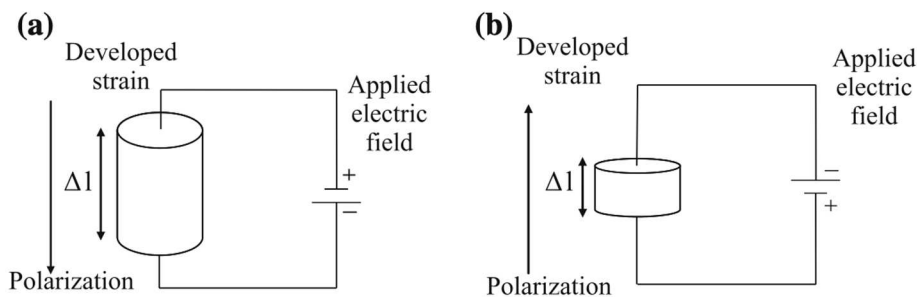


*Fig 2. Inverse piezoelectric effect at applied electric field (Dineva et al., 2014)*

Further investigations on piezoelectric materials (PM) were conducted at that time; one discovery that made an impact on PMs investigations was the discovery of the phenomenon of ferroelectricity by Joseph Valasek (Valasek, 1921). Ferroelectricity on a material is a polar

dielectric that exhibits two or more phases and has a domain structure in which an applied electric field can change polarization (Whatmore, 2017). Rochelle salt was the first ferroelectric material; unfortunately, it was discovered that it loses its ferroelectric properties if the composition changes. The discovery of synthetic materials whose piezoelectric and dielectric were 100 times higher than the materials with natural piezoelectric led to its massive manufacturing.

Piezoelectricity availability on the market was until 1945 when it was realized that the mixed oxide compound barium titanate ( $\text{BaTiO}_3$ ) was a ferroelectric capable of easily being fabricated at a low price; also, its capability of making piezoelectric with constants 100 times higher than natural materials by electric poling. After the piezoelectric effect was a successful application between the two World Wars, piezoelectric ceramics were implemented in many applications. Inkjet printers, medical imaging, and lighters are some of the most common devices used by society; all these devices were created based on the piezoelectric effect.

### **2.3 Piezoelectric Materials**

Piezoelectricity on a material depends on two factors: the material's atomic structure and how electric charge is distributed within it. There are different types of piezoelectric materials, some of them form naturally, and others are manufactured. Natural piezoelectric energy materials are crystal materials, like quartz ( $\text{SiO}_2$ ), Rochelle salt, topaz, and Tourmaline-group minerals; also, there are organic substances that have piezoelectricity, like bone, DNA, and enamel; Figure 3 shows organic materials. Crystals that are quartz analogs, ceramics, polymers, and composite are non-organic PM (Dineva et al., 2014).

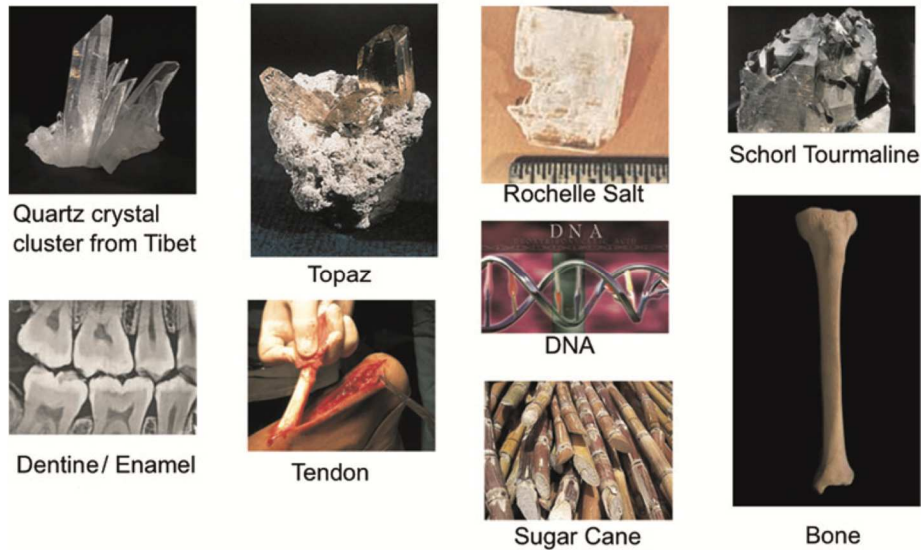


*Fig 3. Natural Piezoelectric materials (Manbachi & Cobbold, 2011)*

It can be found that many materials are crystalline, meaning that these crystal materials (CM) are made of atoms or ions arranged in an orderly three-dimensional pattern. The characteristic of that pattern is that it has a building block called a unit cell. One characteristic that almost all non-piezoelectric CMs have is that the atoms in their unit cells are distributed symmetrically around the center point, but CMs that do not possess a center of symmetry can be classified as CMs with piezoelectricity (Tilley, 2020).

A wide variety of crystals exist; they can be divided into seven groups associated with the elastic nature of the material: triclinic, monoclinic, orthorhombic, tetragonal, trigonal, hexagonal, and cubic (Whatmore, 2017), shown in Figure 4. Out of the thirty-two classes of crystals, only twenty possess piezoelectric properties. Ten are polar; for these, there is no need for mechanical stress to have polarization; this can happen due to a non-vanishing electric dipole associated with

their unit cell. The other ten crystals are not polar, meaning that polarization only occurs when there is a mechanical force applied (Dineva et al., 2014; Kong et al., 2014).

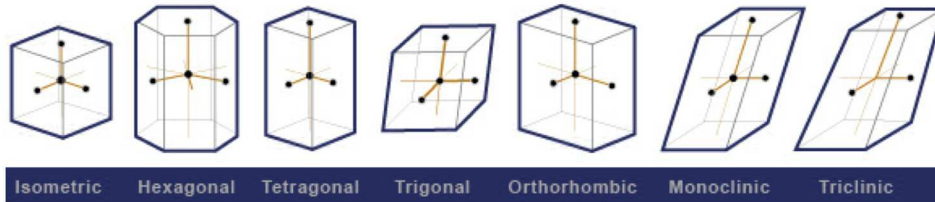


Figure 4. The seven groups of crystals (KHI, 2007).

The mechanism in which these PMs operates is that since they possess a non-centrosymmetric crystal structure, they are able to generate displacement between anions (negatively charged) and cations (positively charged); in many molecules, the separation of these is known as a dipole (a pair of equal and oppositely charged or magnetized poles separated by a distance) moment and typically shown as a vector extending from negative charge to positive charge (Manbachi & Cobbold, 2011). The vector summation of all the dipole moments per volume of the crystal is the dipole density for a medium electric polarization (Birkholz, 1995). Typically, piezoelectric crystals are electrically neutral, meaning that the electric charges are balanced, as shown in Figure 5 a, but if a PM is stretched or squeezed, the structure deforms, as shown in Figures 5 b and c. Atoms will shift along a certain direction, and due to the asymmetry in charge distribution, the dipoles will no longer cancel each other out, causing a net negative charge and a net positive on the other side. A balanced charge is distributed through all the material, and a negative and positive charge collects on opposite faces of the crystal, generating a voltage able to drive electricity through a circuit, as shown in Figure 6.

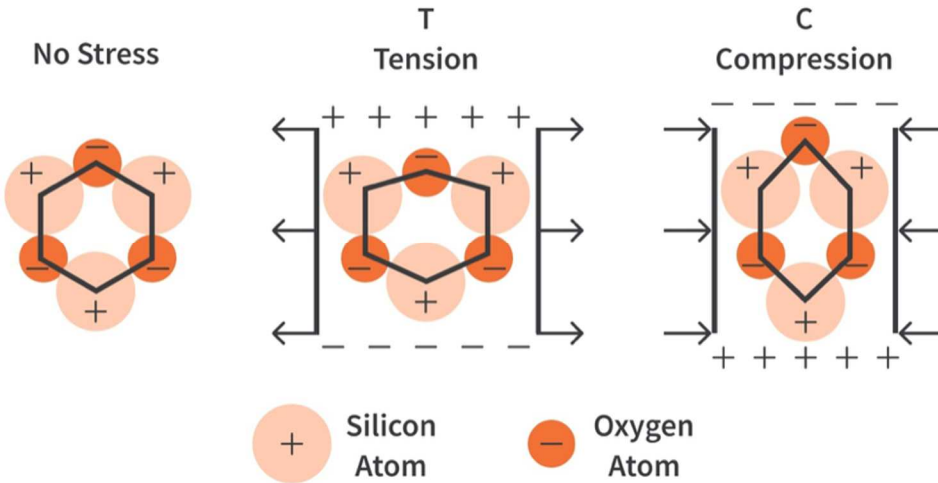


Figure 5. Dipole of Piezoelectric effect in Quartz a) no stress, b) applying tension, c) applying compression (Susie Maestre, 2022)

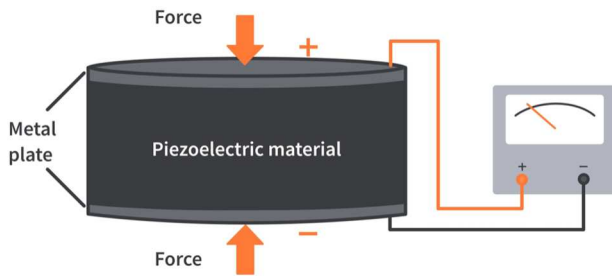


Figure 6. Direct Piezoelectric Effect. Opposite faces with a different charge due to compression of the material (Susie Maestre, 2022)

Among all kinds of piezoelectric materials, there are manufactured polycrystalline (solids that consist of many tiny crystals) piezoelectric materials composed of multiple ferroelectric particles. The following are manufactured ceramics with crystal structure as perovskite: Barium titanate ( $\text{BaTiO}_3$ ), Lead titanate ( $\text{PbTiO}_3$ ), Lead zirconate titanate ( $\text{Pb}[\text{Zr}_x\text{Ti}_{1-x}]\text{O}_3$ ,  $0 < x < 1$ ) – commonly known as PZT, Potassium niobate ( $\text{KNbO}_3$ ), Lithium niobate ( $\text{LiNbO}_3$ ), Lithium tantalate ( $\text{LiTaO}_3$ ), and other lead-free piezoceramics. Lead zirconate titanate (PZT) is

commonly used due to its high piezoelectric charge constant ( $d_{31}$ ,  $d_{33}$ , and  $d_{51}$ ), while other materials are used for microelectromechanical harvesters.

Piezoelectric ceramics are prepared by mixing fine powders in specific portions, then heated to form a uniform powder. The powder is mixed with an organic binder and formed into structural elements; to subsequently fire the elements for a specific time and temperature, where the powder particles sinter and the material obtains a dense crystalline structure. Once the element is entirely cooled, it can be trimmed or shaped, and electrodes can be applied to the appropriate surface. All these ceramics have been extensively studied, and it was demonstrated their effectiveness and efficient building blocks for converting mechanical energy into electricity (Anton & Sodano, 2007; Klimiec et al., 2008; Sun, Xu, & Qi, 2009; Wang, Xudong, Song, Liu, & Wang, 2007; Wang, Zhaoyu, Hu, Suryavanshi, Yum, & Yu, 2007)

## 2.4 Principles of Piezoelectric Effect

The already two mentioned types of piezoelectric effect: direct and reverse effect, as shown in Fig 7. The direct effect was the first discovered phenomenon in which an electric charge is generated from mechanical stress; on the other hand, the reverse effect is related to the mechanical movement induced by applying an electric field. PM characteristics are generally represented by  $d$ ,  $g$ , and  $k$ . The  $d$  factor is called the piezoelectric charge coefficient, including  $d_{31}$  and  $d_{33}$ . Factor  $d_{31}$  is associated with polarization generated in the electrodes perpendicular to the 3-direction when mechanical stress is applied on the 1-direction. Factor  $d_{33}$  is associated with the generation of polarization in the 3-direction when stress is applied along the same direction.

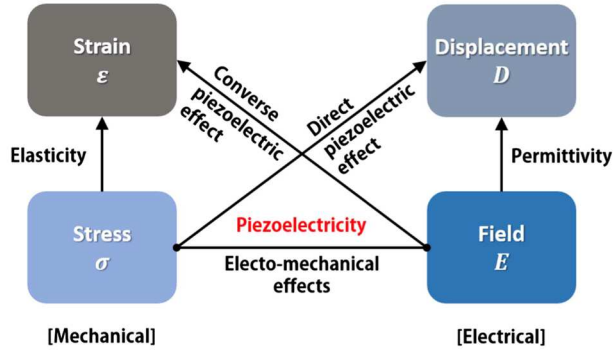


Figure 7. Electromechanical coupling of piezoelectric effect (Song, 2019)

The  $g$  factor, including  $g_{31}$  and  $g_{33}$  represent the piezoelectric voltage coefficient, which are involved in the assessment of the capability of piezoelectric materials to produce voltage per unit area stress; the  $g$  factor can be expressed along with the  $d$  factor as the equation below.

$$g = \frac{d}{K e_0} \quad (1)$$

$e_0$  is the permittivity constant of free space, given as  $8.85 \times 10^{-12}$  F/m, and  $k$  is a free dielectric material parameter.

The  $k$  e.g.,  $k_{31}$ ,  $k_{33}$ , and  $k_p$  are the piezoelectric coupling coefficients; these are used as an index of the conversion efficiency of the piezoelectric materials. The planar coupling factor  $k_p$  indicates radial coupling, which means the coupling between the effect of the mechanical field. The  $k_p$  value can be determined via the resonance and the antiresonance value method; it can be calculated as follow:

$$k_p \cong \sqrt{2.51 \frac{(f_a - f_r)}{f_a}} \quad (2)$$

Where,  $f_a$  and  $f_r$  = antiresonant frequencies and resonant frequencies

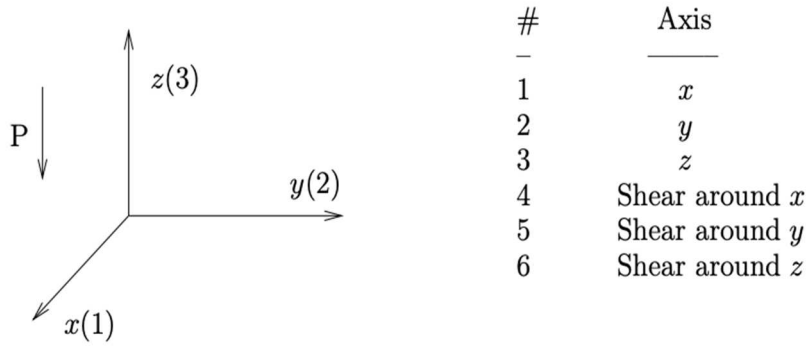


Figure 8. Axis for constitutive equation sample (Moheimani & Fleming, 2006)

The constitutive equations that describe the electromechanical properties of piezoelectric materials will be introduced in this section. These equations are based on the IEEE standard for piezoelectricity (Rosen, Hiremath, & Newnham, 1992). The IEEE standard assumes that the piezoelectric materials are linear. The constitutive equations describing the piezoelectric property are based on the assumption that the total strain on the transducer is the sum of the mechanical stress and the controlled actuation strain caused by the applied voltage. Axis 3 is assigned to the direction of the initial polarization of the piezoceramic, and axes 1 and 2 lie on the plane, as shown in Figure 8.

The describing electromechanical equations for a linear piezoelectric material can be written as

$$\varepsilon_i = S_{ij}^E \sigma_j + d_{mi} E_m \quad (3)$$

$$D_m = d_{mi} \sigma_i + \xi_{ik}^\sigma E_k \quad (4)$$

Where  $i$  and  $j = 1, 2, \dots, 6$  and  $m, k = 1, 2, 3$  refer to the different directions with the material coordinate system, as shown in Figure 8. The above equations can also be written in the following form, which are often used for applications that involve sensing.

$$\varepsilon_i = S_{ij}^D \sigma_j + g_{mi} D_m \quad (5)$$

$$E_i = g_{mi} \sigma_i + \beta_{ik}^\sigma D_k \quad (6)$$

Equations 1 and 2 express the converse piezoelectric effect, which describes the situation when a device is being used as an actuator. Equations 3 and 4 express the direct piezoelectric effect, which is when a transducer is used as a sensor. The converse effect is often used to determine the piezoelectric coefficients. Equations 1 – 4 can be written as

$$\begin{bmatrix} \varepsilon_1 \\ \varepsilon_2 \\ \varepsilon_3 \\ \varepsilon_4 \\ \varepsilon_5 \\ \varepsilon_6 \end{bmatrix} = \begin{bmatrix} S_{11} S_{12} S_{13} S_{14} S_{15} S_{16} \\ S_{21} S_{22} S_{23} S_{24} S_{25} S_{26} \\ S_{31} S_{32} S_{33} S_{34} S_{35} S_{36} \\ S_{41} S_{42} S_{43} S_{44} S_{45} S_{46} \\ S_{51} S_{52} S_{53} S_{54} S_{55} S_{56} \\ S_{61} S_{62} S_{63} S_{64} S_{65} S_{66} \end{bmatrix} \begin{bmatrix} \sigma_1 \\ \sigma_2 \\ \sigma_3 \\ \sigma_4 \\ \sigma_5 \\ \sigma_6 \end{bmatrix} + \begin{bmatrix} d_{11} d_{21} d_{31} \\ d_{12} d_{22} d_{32} \\ d_{13} d_{23} d_{33} \\ d_{14} d_{24} d_{34} \\ d_{15} d_{25} d_{35} \\ d_{16} d_{26} d_{36} \end{bmatrix} \begin{bmatrix} E_1 \\ E_2 \\ E_3 \end{bmatrix} \quad (7)$$

$$\begin{bmatrix} D_1 \\ D_2 \\ D_3 \end{bmatrix} = \begin{bmatrix} d_{11} d_{12} d_{13} d_{14} d_{15} d_{16} \\ d_{21} d_{22} d_{23} d_{24} d_{25} d_{26} \\ d_{31} d_{32} d_{33} d_{34} d_{35} d_{36} \end{bmatrix} \begin{bmatrix} \sigma_1 \\ \sigma_2 \\ \sigma_3 \\ \sigma_4 \\ \sigma_5 \\ \sigma_6 \end{bmatrix} + \begin{bmatrix} e_{11}^\sigma e_{12}^\sigma e_{13}^\sigma \\ e_{21}^\sigma e_{22}^\sigma e_{23}^\sigma \\ e_{31}^\sigma e_{32}^\sigma e_{33}^\sigma \end{bmatrix} \begin{bmatrix} E_1 \\ E_2 \\ E_3 \end{bmatrix} \quad (8)$$

If the device is assumed to be poled along axis 3, and the piezoelectric material is a transversely isotropic material, which is valid for the piezoelectric ceramics. A lot of the parameters in the above matrices will be zero, and the non-zero piezoelectric strain constants would be:

$$d_{31} = d_{32}$$

And

$$d_{15} = d_{24}$$

The non-zero dielectric coefficients are,  $e_{11}^\sigma = e_{22}^\sigma$  and  $e_{33}^\sigma$ . Subsequently, equations 7 and 8 are simplified to:

$$\begin{bmatrix} \varepsilon_1 \\ \varepsilon_2 \\ \varepsilon_3 \\ \varepsilon_4 \\ \varepsilon_5 \\ \varepsilon_6 \end{bmatrix} = \begin{bmatrix} S_{11}S_{12}S_{13} & 0 & 0 & 0 & 0 & 0 \\ S_{12}S_{11}S_{13} & 0 & 0 & 0 & 0 & 0 \\ S_{13}S_{13}S_{33} & 0 & 0 & 0 & 0 & 0 \\ 0 & 0 & 0 & S_{44} & 0 & 0 \\ 0 & 0 & 0 & 0 & S_{44} & 0 \\ 0 & 0 & 0 & 0 & 0 & 2(S_{11} - S_{12}) \end{bmatrix} \begin{bmatrix} \sigma_1 \\ \sigma_2 \\ \sigma_3 \\ \sigma_4 \\ \sigma_5 \\ \sigma_6 \end{bmatrix} + \begin{bmatrix} 0 & 0 & d_{31} \\ 0 & 0 & d_{31} \\ 0 & 0 & d_{33} \\ 0 & d_{15} & 0 \\ d_{15} & 0 & 0 \\ 0 & 0 & 0 \end{bmatrix} \begin{bmatrix} E_1 \\ E_2 \\ E_3 \end{bmatrix} \quad (9)$$

And

$$\begin{bmatrix} D_1 \\ D_2 \\ D_3 \end{bmatrix} = \begin{bmatrix} 0 & 0 & 0 & 0 & d_{15} & 0 \\ 0 & 0 & 0 & d_{15} & 0 & 0 \\ d_{31} & d_{31} & d_{33} & 0 & 0 & 0 \end{bmatrix} \begin{bmatrix} \sigma_1 \\ \sigma_2 \\ \sigma_3 \\ \sigma_4 \\ \sigma_5 \\ \sigma_6 \end{bmatrix} + \begin{bmatrix} e_{11}^\sigma & 0 & 0 \\ 0 & e_{11}^\sigma & 0 \\ 0 & 0 & e_{33}^\sigma \end{bmatrix} \begin{bmatrix} E_1 \\ E_2 \\ E_3 \end{bmatrix} \quad (10)$$

The equations are based on the assumption that the total strain in the transducer is the sum of the mechanical strain induced by the mechanical stress. Figure 7 shows the direction of the axis; axis 1 and 2 represent the plane perpendicular to axis 3, which represents the direction of the initial polarization of the piezoceramic.

## 2.5 Shape Optimization of Piezoelectric Energy Harvesting

Piezoelectric Energy harvesting is a promising technique that can cease with the increment of fossil fuels (Xiong & Wang, 2016); it can produce renewable and clean energy from unused or wasted energy. This technique is defined as capturing, accumulating, and storing energy from surrounding energy sources to give it potential use in the future (Kim et al., 2011). There are different potential sources to harvest electrical energy from the environment, like thermal, wind, hydro, and mechanical energy (Fthenakis & Kim, 2009; Jiang et al., 2017; Pacca & Horvath, 2002; Rome et al., 2005). The environmental source that attracts the most attention is mechanical energy due to its independence from weather or season to collect energy (Liao & Sodano, 2008; Liao & Liang, 2018; Yang, Z., Erturk, & Zu, 2017). In particular, PEH is gaining significant research interest due to its simplicity in collecting ambient energy from vehicle vibration (Song et al., 2016; Uzun & Kurt, 2013).

Piezoelectric vibration energy harvesting technology is favored in vibration energy harvesting due to the high electrical conversion coefficient and no external power supply being required. Vibration energy can be obtained from different sources, for example, roads, railroads, buildings, and mechanical equipment (Elvin, Niell & Erturk, 2013; Roshani, Dessouky, Montoya, & Papagiannakis, 2016; Siddique, Mahmud, & Van Heyst, 2015). As previously mentioned, there is an increment of vehicles on roads each year, meaning that there is vibration energy on roads not being used (Cho et al., 2019; Lee & Choi, 2014; Tan et al., 2013; Wang et al., 2016). If road engineering and PVEH technology could be implemented on the most transited roads, there would be more clean and intelligent roads and an effect on the environment.

Research on the electrical conversion of vibrating micro-energy has been popular thanks to Williams and Yates; they were the first to propose the conversion of vibrational energy into

electrical energy in 1996 (Williams & Yates, 1996). Currently, there are two piezoelectric technologies for the pavement to scavenge vibration: piezoelectric material composite power generation pavement technology and transducer embedded pavement piezoelectric power generation technology.

The first technology comprises compounding pavement and piezoelectric materials in road paving to harvest vibration energy. A ductive asphalt layer and a piezoelectric material layer were designed, and the power generation characteristics were verified; a piezoelectric module was used in actual roads, and an output voltage of 7.2 V was achieved (Guo & Lu, 2017b). The preparation of piezoelectric asphalt composites by combining piezoelectric materials and asphalt and generating an output voltage of up to 7.2 V (Tan et al., 2013). The preparation of  $d_{31}$  and  $d_{33}$ , two forms of piezoelectric asphalt concrete, by compounding piezoelectric, conductive, electrode, and pavement materials with an output voltage of up to 2.4 V (Wang et al., 2016)

The second technology consists of embedding piezoelectric transducers into the asphalt pavement to harvest and convert road mechanical energy into energy. There are numerous studies in this area. An example of these studies is where piezoelectric material was optimized, and finite element was used to compare the energy outputs of different transducers in road environment (Cafiso, Cuomo, Di Graziano, & Vecchio, 2013; Najini & Muthukumaraswamy, 2016). An instantaneous output power of up to 200 mW across 40 k $\Omega$  from a PEH module based on polyvinylidene fluoride (Jung, Shin, Kim, Choi, & Kang, 2017). The output power that could reach 0.46 mW from the energy output effect of stacked piezoelectric transducers under different conditions by simulating the typical road load. The construction of LED traffic signal guidance lamp based on piezoelectric cantilever beam transducers after analyzing the feasibility of road

energy harvesting (Collin, 2014). An exploration of the feasibility of transducer-embedded piezoelectric power generation pavement, where it was preliminarily studied the single piezoelectric element buried directly into the pavement and tested the energy output effect; and a maximum voltage of 14 V and an effective power of 0.44 mW were obtained (Chao-hui, Sen, Yan-wei, Xin, & Qing, 2016). Also, another piezoelectric energy harvesting module based on polyvinylidene fluoride exhibited 200 mW of power generation (Kim, K. et al., 2018).

All these research had successful results; all the simulations generated energy using piezoelectric materials. Even though both technologies are being used and studied, the piezoelectric metrical composite power generation pavement has more popularity than transducer-embedded pavement piezoelectric power generation technology, but there are several disadvantages. The major disadvantages include difficult polarization, complex material preparation, low energy output, and lacking of continuous energy supply for real-world application (Wang et al., 2018). The transducer-embedded pavement piezoelectric power generation technology can obtain higher and more controllable output; based on this, the modern technology used in roads to harvest energy is placing piezoelectric transducers directly on pavement structures.

The main concern of piezoelectric energy harvesters is the low energy production and the sustainable energy supply. Different researchers have studied the improvement of the piezoelectric energy harvester's structure. To improve power density, a rectangular cantilever harvester was shaped into a triangular and trapezoidal shape (Baker, Roundy, & Wright, 2005; Muthalif & Nordin, 2015). A flexible longitudinal zigzag structure to harvest low-frequency vibration energy (Zhou, S., Chen, Malakooti, Cao, & Inman, 2017). The design of a multilayer stacked PEH; in this design, the flex-tensional force was taken into consideration and achieved

as high as 26% mechanical to electrical energy conversion efficiency (Xu, Jiang, & Su, 2011). The study of a bi-stable composite structure with a layer of curved steel and a flat piezo fiber laminate (Giddings, Kim, Salo, & Bowen, 2011). A cymbal transducer made of two concave-shaped metal endcaps and one flat piezoelectric disc was made to harvest more energy from excitations with a large amplitude force (Kim, H. W. et al., 2004). The fabrication of a compressive-mode PEH using a flexural structure and bending beams could generate over 20 milliwatts of power under a 0.2g ( $g = 9.8 \text{ m/s}^2$ ) weak excitation (Yang, Z. & Zu, 2014; Yang, Z., Zhu, & Zu, 2015). The study of an M-shaped structure with a bent spring steel and flat PZT patches (Leadenham & Erturk, 2015).

CHAPTER III  
METHODOLOGY

**3.1 Finite Element Analysis**

In the past, the only way to develop improvements on electro-acoustic transducers was primarily by trial and error; this process could be time-consuming and expensive at the same time. The trial-and-error practice is not consistent with modern industrial engineering practice, which is computer simulations to aid the development of transducers. The primary purpose of computer simulations in transducer development is to optimize the transducer design without time-consuming experiments, deeper insight into the wave propagation in piezoelectric solids, and evaluation of new materials in device design.

Finite element analysis (FEA) has become an integral part of the design and development of numerous engineering systems. The FEA is a numerical method used to obtain an approximate solution for a given boundary problem; it takes the boundary value problem and converts it into a linear system of equations. During the design of a structure, two main components must be considered. One, the high degree of integration of sensors, actuators, and structures requires techniques of modeling hybrid material systems. Second, its multidisciplinary to be designed. To design smart structures, accurate structural modeling is not enough; it requires both structural dynamics and control theory to be considered. FEA is widely accepted for its capacity to analyze complex structures, complex problems, complex restraints, complex loading

conditions, Multiphysics (thermomechanical, electromechanical, and so on). This method deals with the integration of smart components and classic structural parts; unique finite elements have been developed to account for the piezoelectric effect (Benjeddou, 2000); also, piezoelectric elements have become available in commercial finite element codes such as ABAQUS/Standard.

Several studies about piezoelectric sensing and actuation use FEM for plates with piezoelectric materials. FEM and formulation for modeling of piezoelectric cantilever have been a crucial problem for several studies (Bendary, Elshafei, & Riad, 2010a; Elvin, Niell G. & Elvin, 2009; Yang, Y. & Tang, 2009). It was reported, as verified by the analytical and experimental results in the literature, that an improvement on the finite element model by adding conductive electrodes based on Hamilton's principle (Junior, Erturk, & Inman, 2009). The formulation of a distributed couple electromechanical model that represents the static and dynamic behavior of the PTZ device (Bendary, Elshafei, & Riad, 2010b). All the mentioned studies had success in modeling PZT cantilever beams for energy generation, meaning that the FEM is an accurate solution to model PEH.

ABAQUS is a finite element program designed for structural and heat transfer analysis. It is designed to solve linear and nonlinear stress analysis for any structure dimension. The software provides a complete element library that provides a geometric modeling capability. Beams, shells, solids, and pipes with one, two, and three dimensions; also, be modeled using first, second, or third order interpolation. There is a built-in automatic adaptive choice of time incrementation, meaning that it can provide uniform accuracy throughout the solution (Giner, Sukumar, Tarancón, & Fuenmayor, 2009)

### 3.2 Finite Element Modeling

For this study, ABAQUS/standard software was used to create different PEH models. The models were created based on the unimorph energy harvester design in (Song, 2019). The REC model has the exact dimensions as the one created in the study, shown in Figure 9. Models L1-R3 and L3-R1 were designed based on this model; the difference is that these models have a trapezoidal shape, as shown in Figures 10, 11, and 12. Table 1 shows the exact dimensions used in the models.

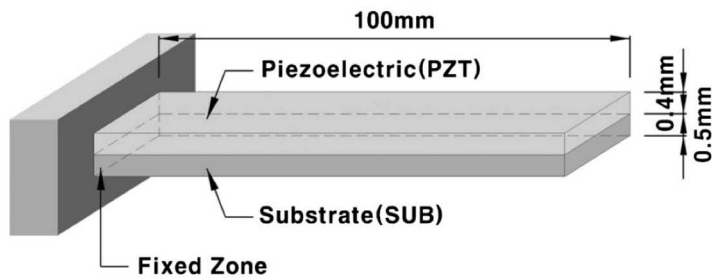


Figure 9. Energy harvester geometry and dimensions (Song, 2019)

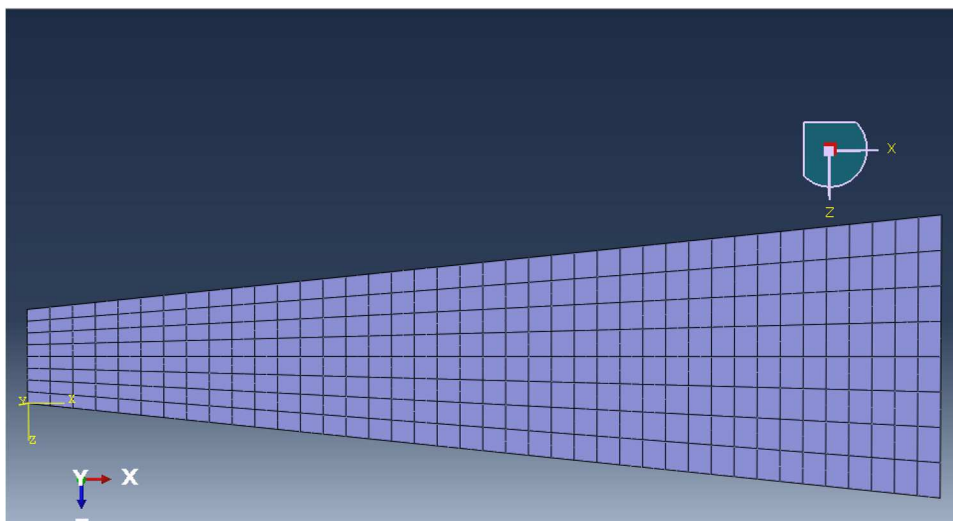


Figure 10. Top view of model L1-R3

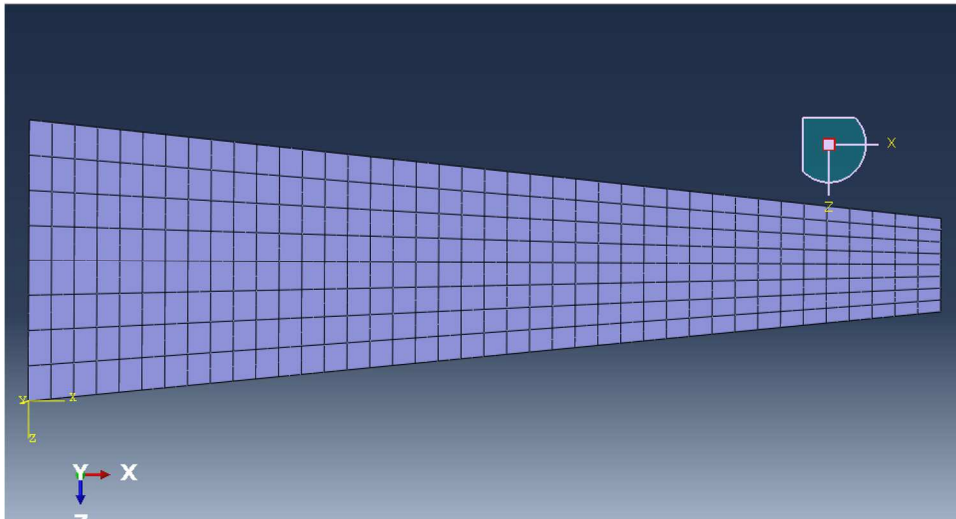


Figure 11. Top view of model L3-R1

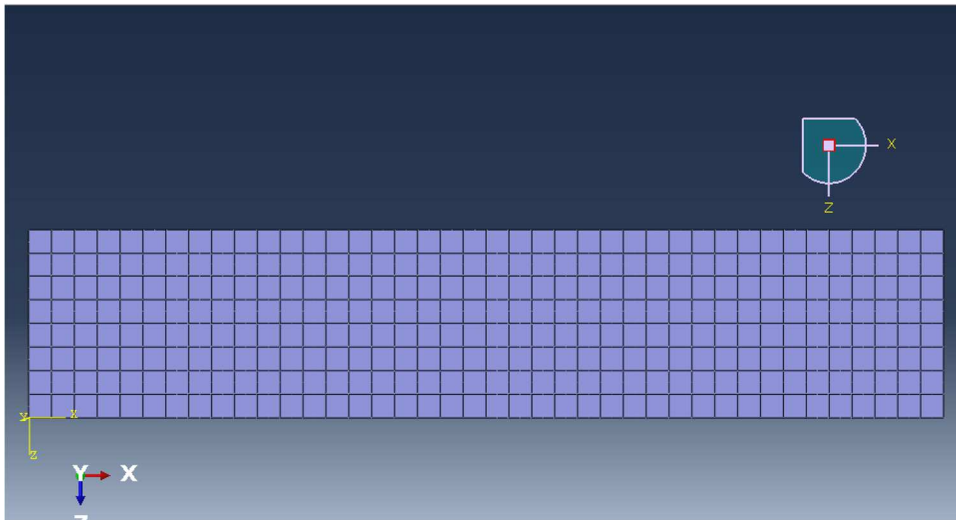


Figure 12. Top view of model REC

*Table 1. Dimensions of PEHs*

Model	L1-R3	R3-L1	REC
Length	10 cm	10 cm	10 cm
Width	Short side :1 cm Long side: 3 cm	Short side :1 cm Long side: 3 cm	2 cm
Thickness	PZT: 4 mm Substructure: 5mm	PZT: 4 mm Substructure: 5mm	PZT: 4 mm Substructure: 5mm
Area	20 cm <sup>2</sup>	20 cm <sup>2</sup>	20 cm <sup>2</sup>

To create the PEH models, a solid homogeneous geometry was created. The structure consists of a PZT layer at the top and a substructure at the bottom. Both layers have the exact measurements, except for the thickness, as shown in Table 1. There are three models, one rectangle and two trapezoids; the difference is in the width of the structure for the trapezoids. The purpose of having the same area is that the results depend on the structure shape and not on the area. The properties of each material used for each layer are shown in Table 2

*Table 2. Material Properties for the PEHs*

Property	Piezoelectric	Substructure
Elastic Modulus for isotropic linear elasticity, Y (GPA)	66	100
Density, $\rho$ (g * cm <sup>3</sup> )	7.8	7.165
Piezoelectric Charge coefficient d31 (pm/V)	-190	
Dielectric Permittivity at constant stress, $\epsilon_{33}$ (nF/m)	15.93	
Beta	4.885	4.885
Alpha	1.24E-06	1.24E-06

It was assumed that a perfectly conductive electrode completely coats each finite element on the top and bottom surfaces, and a single electric DOF was adequate to simulate the electric behavior. After each material's properties were assigned, the mesh was created. For the PZT, the mesh element type was C3D20E: A 20-node quadratic piezoelectric brick, and C3D20: A 20-

node quadratic brick for the substructure; with an approximate global size of 0.0025, creating a total of 320 elements, and 2,483 nodes on each layer. The two layers were assembled to create one single structure.

The boundary conditions for the structure were set, as shown in figure 11. The Boundary conditions DISP-BC-1 and DISP-BC-2 were placed on the PZT layer left side of the structure, and the EEC-BC-3 was set on the bottom nodes of the PZT layer. The result of all the properties applied to the structure are shown in Figure 13; the yellow arrows indicate the amplitude applied to the structure, the orange cones are the boundary conditions for displacement and rotation at the side of the structure, and the orange squares are the electric potential at the bottom of the PZT layer, as shown in Figure14.

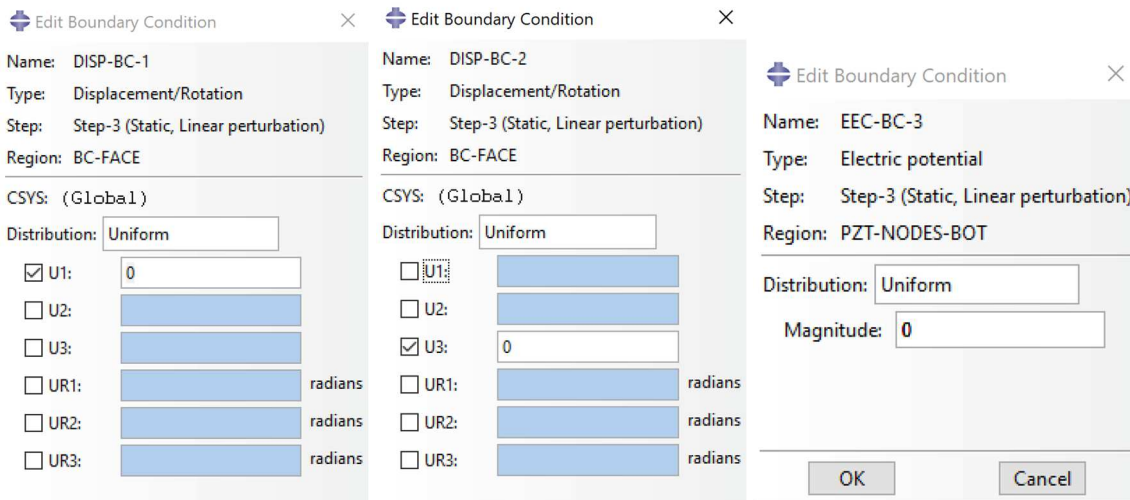
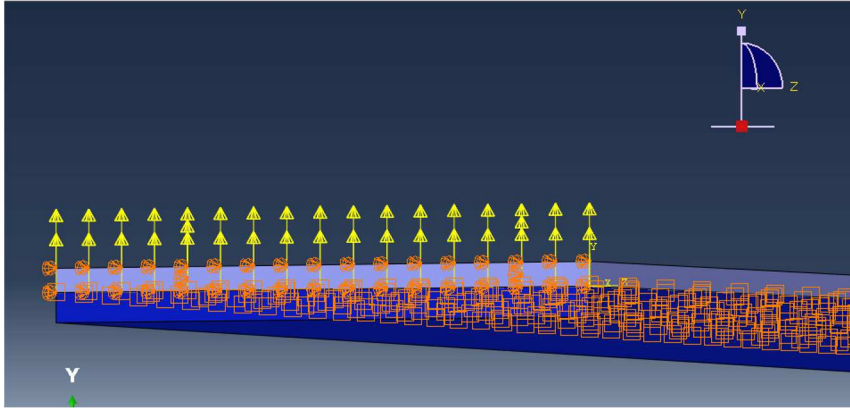


Figure 13. Boundary Conditions for the structure



*Figure 14. Boundary conditions applied to the structure*

### **3.3 Model Validation**

In this section the model created on this study was validated using ABAQUS/Standard, and theoretically. The theoretical validation for the REC model was obtained from the work done by (Song, 2019), where the numerical results from that study were compared with the work of (Erturk & Inman, 2008). To validate the shape of the PEH, the finite element implementation of a unimorph PEH was studied through the commercial software ABAQUS/Standard. In (Song, 2019) the numerical results from the simulations in ABAQUS/Standard of the proposed PEH were compared with the analytical (closed form) solutions originally proposed by (Erturk & Inman, 2008) for a linear system to corroborate the global matrixes of mass, damping, and linear stiffness. The proposed PEH by (Erturk & Inman, 2008) is shown in Figure 8, and the properties of the model are in Table 2.

The numerical results obtained from ABAQUS/Standard in (Song, 2019) study were compared with the theoretical solution given by (Erturk & Inman, 2008), as shown in Figure 15, and Table 3. The results obtained demonstrated excellent agreement with the analytical solution.

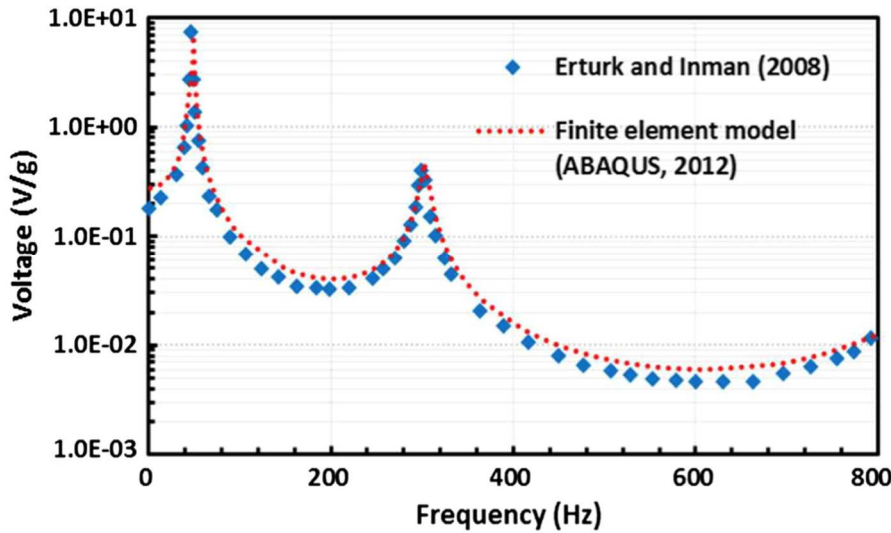


Figure 15. Model validation from (Song, 2019).

Table 3. First and second modes of natural frequencies for theoretical validation (Hz) (Song, 2019)

Property	Piezoelectric	Substructure
(Erturk & Inman, 2008)	47.80	299.60
ABAQUS/Standard	47.68	302.28

In the study, the researchers obtain the voltage using finite element simulations with ABAQUS subjected to a unit force at the designated measurement points on a single-span bridge. The simulations were performed at seven different train speeds, 100 km/h, 200 km/h, 250 km/h, 300 km/h, 330 km/h, and 350 km/h. Once the vertical acceleration was obtained from the different speeds. Figure 16 shows the schematic of the setup used for the finite element simulations indicating the measurement points from which the vibration response data was generated.

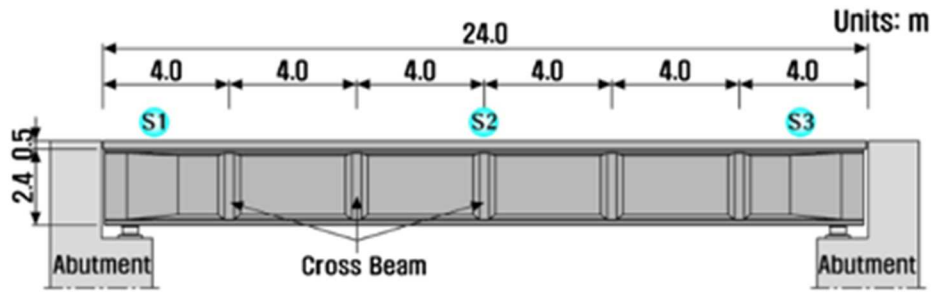


Figure 16. Schematic for the points where the voltage was obtained (Song, 2019)

For this study, the voltage obtained from the study (Song, 2019) was compared with this study to know if the model would create voltage. The results obtained from the ABAQUS/Standard simulation in this study would demonstrate if voltage can increase depending on the PEH shape.

## CHAPTER IV

### RESULTS

The models created on ABAQUS/standard demonstrated an output voltage in each model at different speeds obtained from (Song, 2019). The output voltage generated in each model is shown in Figure 18. The results were then compared on an RMS graph to find the shape that harvested the most energy, as shown in Figure 17. The results from this research were compared with those from (Song, 2019), as shown in Figure 19.

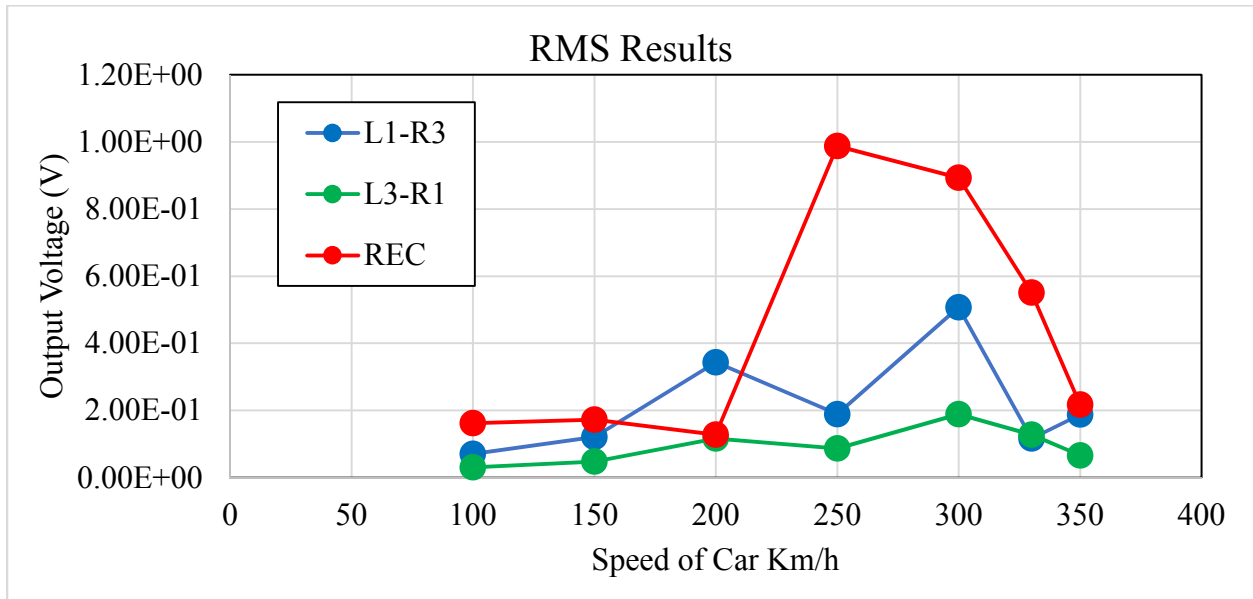
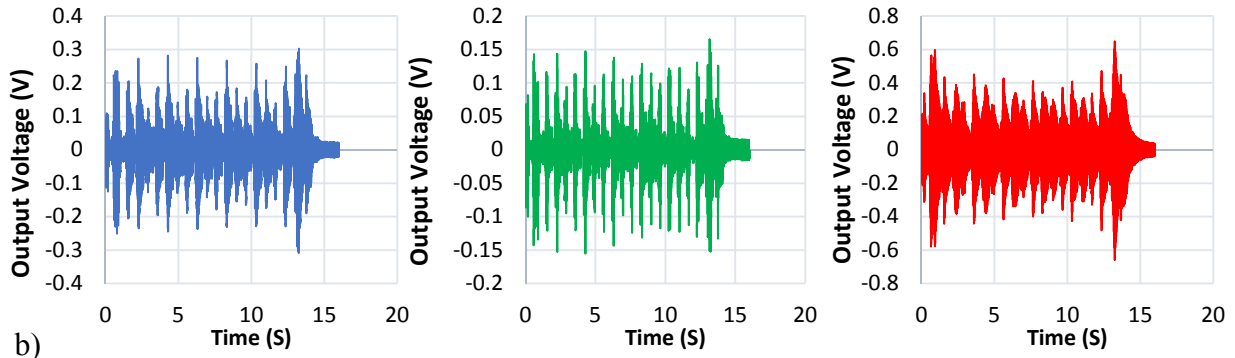
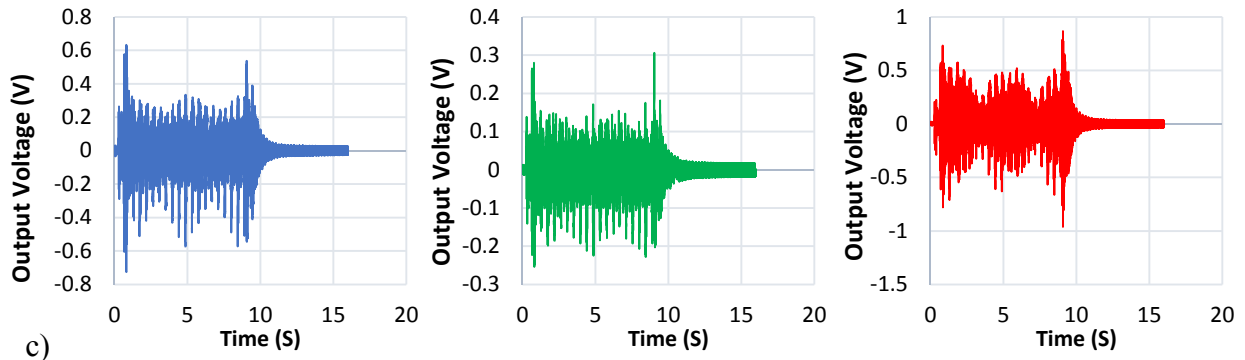


Figure 17. RMS results at different speeds.

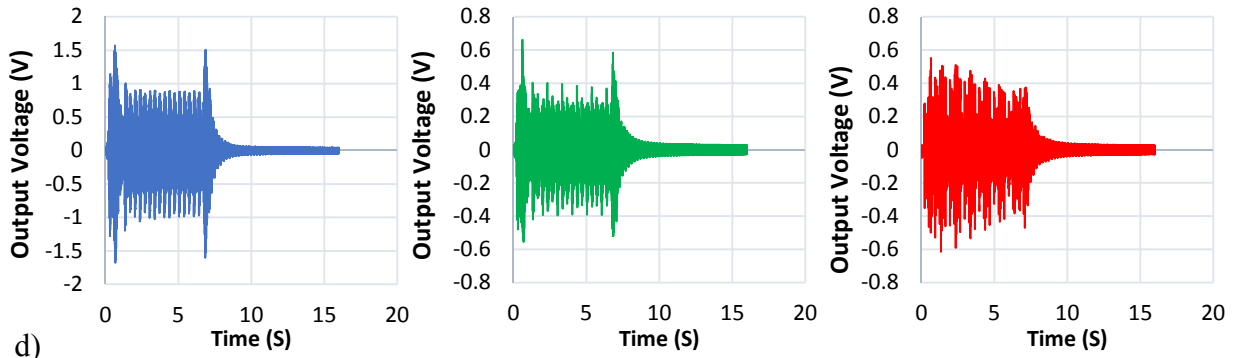
a)



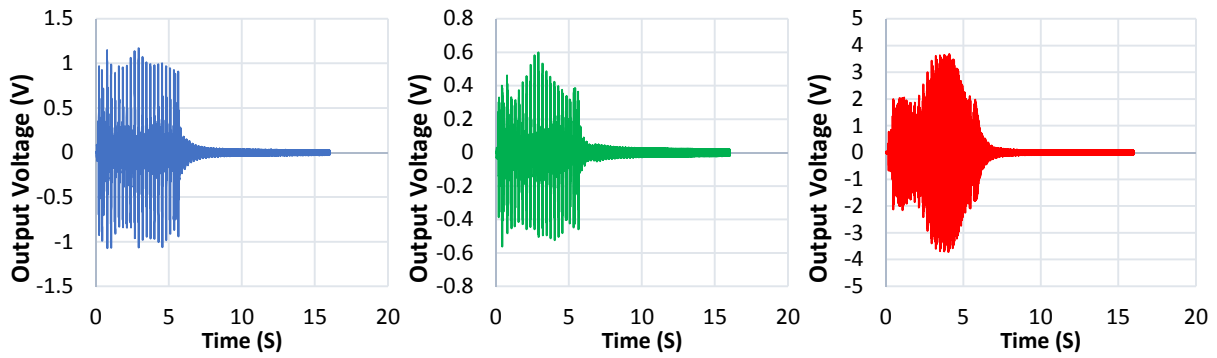
b)



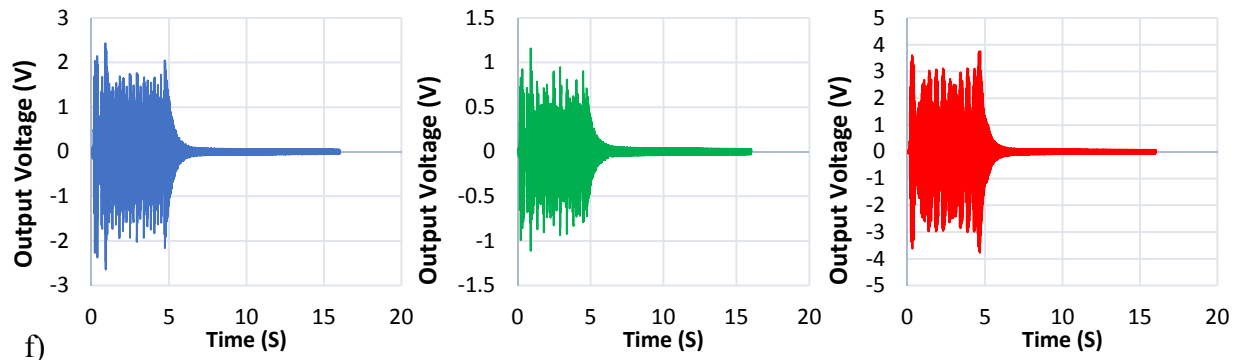
c)



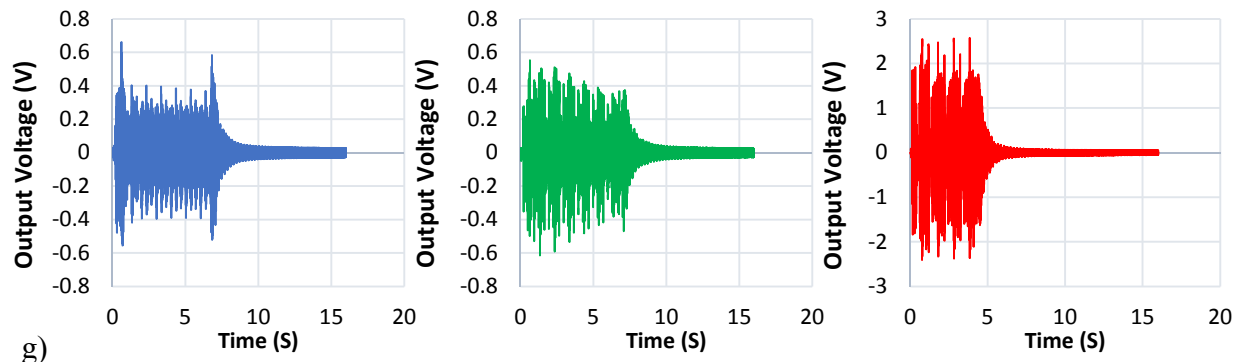
d)



e)



f)



g)

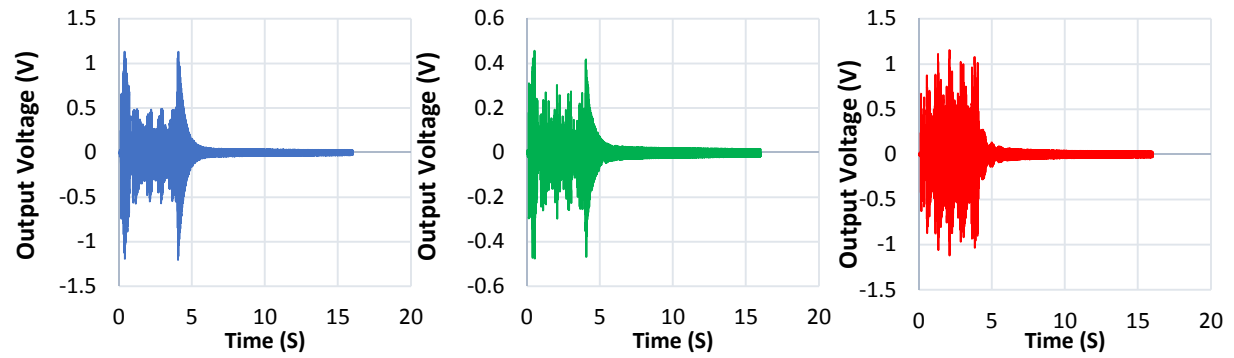


Figure 18. Output Voltage from the PEHs a) 100 km/h b) 150 km/h, c) 200

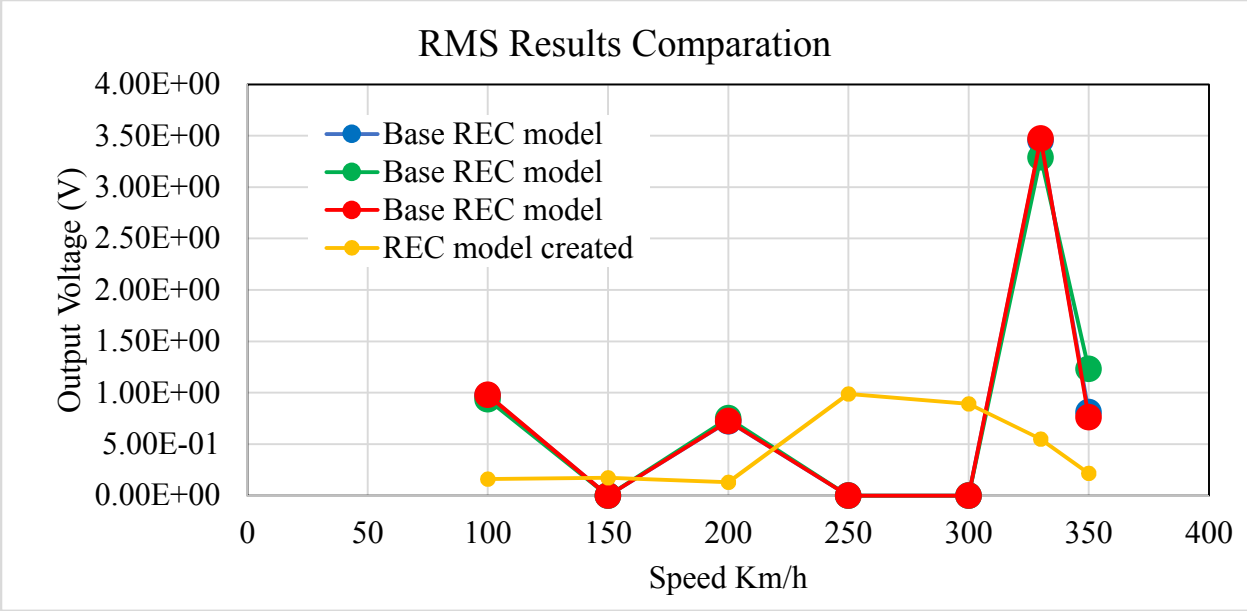


Figure 19. REC model comparison

## CHAPTER V

### ANALYSIS

The models created in this research were based on the validated model from (Song, 2019); from the results obtained, it was shown that the models generated an output voltage, which means that the model was correctly created on ABAQUS/Standard. Also, a comparison with the base model results was made, as shown in Figure 19. Even though the results are different, it can be said that the model works because the original model was created with an excitation mass at the tip of the harvester, and the one created in this study did not. The models were then compared on an RMS graph with each other to find the shape that generated more voltage; as it is shown in Figure 17, from the graph, it can be concluded that the shape with the most significant output voltage is the REC model. The REC model was the only shape with a high increment as the speed changed, compared with the other two models.

In the literature review section, several studies demonstrated that the shape design of PEHs impacts output voltage; by comparing this study with other studies, it can be concluded that the shape influences the output voltage.

## CHAPTER VI

### CONCLUSION

Piezoelectric energy harvesting technology on roads is an important subject that needs to be studied due to its impact on society. PEHs can generate clean energy from waste vibrations on roads. This study investigated a PEH system subjected to mechanical vibrations using ABAQUS/Standard. The dimensions and properties of a validated model were used to create three different PEH models to find if shape optimization is a factor in energy harvesting. The three models were then tested at different speeds to find the output voltage of each shape. The results obtained showed different output voltages in each of the models; based on the results in this research, it can be concluded that shape optimization on PEHs has an impact on energy harvesting.

## REFERENCES

- ABAQUS Online Documentation. (2006). ABAQUS theory manual. Retrieved from <https://classes.engineering.wustl.edu/2009/spring/mase5513/abaqus/docs/v6.6/books/stm/default.htm?startat=book01.html#stm>
- Anton, S. R., & Sodano, H. A. (2007). A review of power harvesting using piezoelectric materials (2003–2006). *Smart Materials and Structures*, 16(3), R1.
- Arnau, A., & Soares, D. Fundamentals of piezoelectricity. *Piezoelectric transducers and applications* (pp. 1-38). Berlin, Heidelberg: Springer Berlin Heidelberg. doi:10.1007/978-3-540-77508-9\_1 Retrieved from [http://link.springer.com/10.1007/978-3-540-77508-9\\_1](http://link.springer.com/10.1007/978-3-540-77508-9_1)
- Baker, J., Roundy, S., & Wright, P. (2005). Alternative geometries for increasing power density in vibration energy scavenging for wireless sensor networks. Paper presented at the *3rd International Energy Conversion Engineering Conference*, 5617.
- Bendary, I. M., Elshafei, M. A., & Riad, A. M. (2010a). Finite element model of smart beams with distributed piezoelectric actuators. *Journal of Intelligent Material Systems and Structures*, 21(7), 747-758.
- Bendary, I. M., Elshafei, M. A., & Riad, A. M. (2010b). Finite element model of smart beams with distributed piezoelectric actuators. *Journal of Intelligent Material Systems and Structures*, 21(7), 747-758.
- Benjeddou, A. (2000). Advances in piezoelectric finite element modeling of adaptive structural elements: A survey. *Computers & Structures*, 76(1-3), 347-363.
- Birkholz, M. (1995). Crystal-field induced dipoles in heteropolar crystals II: Physical significance. *Zeitschrift Für Physik B Condensed Matter*, 96(3), 333-340.
- BP. (2021). *Statistical review of world energy 2021 | 70th edition*. (). Retrieved from <https://www.bp.com/content/dam/bp/business-sites/en/global/corporate/pdfs/energy-economics/statistical-review/bp-stats-review-2021-full-report.pdf>
- Cafiso, S., Cuomo, M., Di Graziano, A., & Vecchio, C. (2013). Experimental analysis for piezoelectric transducers applications into roads pavements. Paper presented at the *Advanced Materials Research*, , 684 253-257.

- Chao-hui, W., Sen, C., Yan-wei, L. I., Xin, S., & Qing, L. I. (2016). Design of piezoelectric elements' protection measures and energy output of intelligent power pavement. *China Journal of Highway and Transport*, 29(5), 41.
- Cho, J. Y., Kim, K., Hwang, W. S., Yang, C. H., Ahn, J. H., Do Hong, S., . . . Woo, S. B. (2019). A multifunctional road-compatible piezoelectric energy harvester for autonomous driver-assist LED indicators with a self-monitoring system. *Applied Energy*, 242, 294-301.
- Collin, D. (2014). Piezoelectric powered LED street reflector. *California Polytechnic State University, Spring*,
- Delorme, A., Karbowski, D., & Sharer, P. (2010). Evaluation of fuel consumption potential of medium and heavy duty vehicles through modeling and simulation. *Evaluation of Fuel Consumption Potential of Medium and Heavy Duty Vehicles through Modeling and Simulation.*,
- Dineva, P., Gross, D., Müller, R., & Rangelov, T. (2014). Piezoelectric materials. *Dynamic fracture of piezoelectric materials* (pp. 7-32) Springer.
- Duck, F. A., & Thomas, A. (2022). Paul langevin (1872-1946): The father of ultrasonics. *Medical Physics*, 10(1)
- Duck, F. (2009). 'The electrical expansion of quartz' by jacques and pierre curie. *Ultrasound*, 17(4), 197-203.
- Elvin, N. G., & Elvin, A. A. (2009). A coupled finite element—circuit simulation model for analyzing piezoelectric energy generators. *Journal of Intelligent Material Systems and Structures*, 20(5), 587-595.
- Elvin, N., & Erturk, A. (2013). *Advances in energy harvesting methods* Springer Science & Business Media.
- Erturk, A., & Inman, D. J. (2008). A distributed parameter electromechanical model for cantilevered piezoelectric energy harvesters. *Journal of Vibration and Acoustics*, 130(4)
- Giddings, P. F., Kim, H. A., Salo, A. I., & Bowen, C. R. (2011). Modelling of piezoelectrically actuated bistable composites. *Materials Letters*, 65(9), 1261-1263.
- Giner, E., Sukumar, N., Tarancón, J. E., & Fuenmayor, F. J. (2009). An abaqus implementation of the extended finite element method. *Engineering Fracture Mechanics*, 76(3), 347-368. doi:10.1016/j.engfracmech.2008.10.015
- Guldentops, G., Nejad, A. M., Vuye, C., & Rahbar, N. (2016). Performance of a pavement solar energy collector: Model development and validation. *Applied Energy*, 163, 180-189.

- Guo, L., & Lu, Q. (2017a). Modeling a new energy harvesting pavement system with experimental verification. *Applied Energy*, 208, 1071-1082.
- Guo, L., & Lu, Q. (2017b). Modeling a new energy harvesting pavement system with experimental verification. *Applied Energy*, 208, 1071-1082.
- Highway statistics 2012. federal highway administration. Retrieved from <https://www.fhwa.dot.gov/policyinformation/statistics/2012/>
- Jung, I., Shin, Y., Kim, S., Choi, J., & Kang, C. (2017). Flexible piezoelectric polymer-based energy harvesting system for roadway applications. *Applied Energy*, 197, 222-229. doi:10.1016/j.apenergy.2017.04.020
- Junior, C. D. M., Erturk, A., & Inman, D. J. (2009). An electromechanical finite element model for piezoelectric energy harvester plates. *Journal of Sound and Vibration*, 327(1-2), 9-25.
- Katzir, S. (2006). The discovery of the piezoelectric effect. *The beginnings of piezoelectricity* (pp. 15-64) Springer.
- KHI, I. (2007). Crystalline structures | crystal lattice structures. Retrieved from [https://folk.ntnu.no/yingday/NilsYD/PhaseStructure/Crystal%20Lattice%20\\_%20Crystal%20System.pdf](https://folk.ntnu.no/yingday/NilsYD/PhaseStructure/Crystal%20Lattice%20_%20Crystal%20System.pdf)
- Kim, H. W., Batra, A., Priya, S., Uchino, K., Markley, D., Newnham, R. E., & Hofmann, H. F. (2004). Energy harvesting using a piezoelectric “cymbal” transducer in dynamic environment. *Japanese Journal of Applied Physics*, 43(9R), 6178.
- Kim, K., Cho, J. Y., Jabbar, H., Ahn, J. H., Do Hong, S., Woo, S. B., & Sung, T. H. (2018). Optimized composite piezoelectric energy harvesting floor tile for smart home energy management. *Energy Conversion and Management*, 171, 31-37.
- Klimiec, E., Zaraska, W., Zaraska, K., Gąsiorowski, K. P., Sadowski, T., & Pajda, M. (2008). Piezoelectric polymer films as power converters for human powered electronics. *Microelectronics Reliability*, 48(6), 897-901. doi:10.1016/j.microrel.2008.04.001
- Kong, L. B., Li, T., Hng, H. H., Boey, F., Zhang, T., & Li, S. (2014). Waste mechanical energy harvesting (I): Piezoelectric effect. *Waste energy harvesting* (pp. 19-133) Springer.
- Leadenham, S., & Erturk, A. (2015). Nonlinear M-shaped broadband piezoelectric energy harvester for very low base accelerations: Primary and secondary resonances. *Smart Materials and Structures*, 24(5), 055021.
- Lee, J., & Choi, B. (2014). Development of a piezoelectric energy harvesting system for implementing wireless sensors on the tires. *Energy Conversion and Management*, 78, 32-38.

- Liao, Y., & Liang, J. (2018). Maximum power, optimal load, and impedance analysis of piezoelectric vibration energy harvesters. *Smart Materials and Structures*, 27(7), 075053.
- Liao, Y., & Sodano, H. A. (2008). Model of a single mode energy harvester and properties for optimal power generation. *Smart Materials and Structures*, 17(6), 065026.
- Manbachi, A., & Cobbold, R. S. (2011). Development and application of piezoelectric materials for ultrasound generation and detection. *Ultrasound*, 19(4), 187-196.
- Moheimani, S. R., & Fleming, A. J. (2006). Fundamentals of piezoelectricity. *Piezoelectric Transducers for Vibration Control and Damping*, , 9-35.
- Moure, A., Rodríguez, M. I., Rueda, S. H., Gonzalo, A., Rubio-Marcos, F., Cuadros, D. U., . . . Fernández, J. F. (2016). Feasible integration in asphalt of piezoelectric cymbals for vibration energy harvesting. *Energy Conversion and Management*, 112, 246-253.
- Muthalif, A. G., & Nordin, N. D. (2015). Optimal piezoelectric beam shape for single and broadband vibration energy harvesting: Modeling, simulation and experimental results. *Mechanical Systems and Signal Processing*, 54, 417-426.
- Najini, H., & Muthukumaraswamy, S. A. (2016). Investigation on the selection of piezoelectric materials for the design of an energy harvester system to generate energy from traffic. *International Journal of Engineering and Applied Sciences*, 3(2), 257722.
- Rosen, C., Hiremath, B. V., & Newnham, R. (1992). *Piezoelectricity* Springer Science & Business Media.
- Roshani, H., Dessouky, S., Montoya, A., & Papagiannakis, A. T. (2016). Energy harvesting from asphalt pavement roadways vehicle-induced stresses: A feasibility study. *Applied Energy*, 182, 210-218.
- Siddique, A. R. M., Mahmud, S., & Van Heyst, B. (2015). A comprehensive review on vibration based micro power generators using electromagnetic and piezoelectric transducer mechanisms. *Energy Conversion and Management*, 106, 728-747.
- Song, Y. (2019). Finite-element implementation of piezoelectric energy harvesting system from vibrations of railway bridge. *Journal of Energy Engineering*, 145(2), 04018076.
- Sun, F. M., Xu, X. S., & Qi, Z. H. (2009). Non-linear vibration and dynamic characteristic of fish-like robot controlled by GMM actuator. *Journal of Intelligent Material Systems and Structures*, 20(12), 1503-1513.
- Susie Maestre. (2022). What is piezoelectric effect? Retrieved from <https://www.circuitbread.com/ee-faq/what-is-piezoelectric-effect>

- Tan, Y. Q., Zhong, Y., Lv, J., Ouyang, J., & Zhou, S. (2013). Preparation and properties of PZT/asphalt-based piezoelectric composites used on pavement. *J Build Mater*, 16(6), 975-980.
- Tilley, R. J. (2020). *Crystals and crystal structures* John Wiley & Sons.
- Uchino, K. (2017). Chapter 1 - the development of piezoelectric materials and the new perspective. In K. Uchino (Ed.), *Advanced piezoelectric materials (second edition)* (pp. 1-92) Woodhead Publishing. doi:<https://doi.org/10.1016/B978-0-08-102135-4.00001-1>  
Retrieved from <https://www.sciencedirect.com/science/article/pii/B9780081021354000011>
- Valasek, J. (1921). Piezo-electric and allied phenomena in rochelle salt. *Physical Review*, 17(4), 475.
- Wang, C. H., Wang, H. L., & Li, Y. (2016). Study on technology of power pavement based on integration of piezoelectric material and pavement material. *J Highw Transp Res Dev*, 33(11), 14-19.
- Wang, C., Zhao, J., Li, Q., & Li, Y. (2018). Optimization design and experimental investigation of piezoelectric energy harvesting devices for pavement. *Applied Energy*, 229, 18-30.
- Wang, X., Song, J., Liu, J., & Wang, Z. L. (2007). Direct-current nanogenerator driven by ultrasonic waves. *Science*, 316(5821), 102-105.
- Wang, Z., Hu, J., Suryavanshi, A. P., Yum, K., & Yu, M. (2007). Voltage generation from individual BaTiO<sub>3</sub> nanowires under periodic tensile mechanical load. *Nano Letters*, 7(10), 2966-2969.
- Whatmore, R. (2017). Ferroelectric materials. *Springer handbook of electronic and photonic materials* (pp. 1) Springer.
- Williams, C. B., & Yates, R. B. (1996). Analysis of a micro-electric generator for microsystems. *Sensors and Actuators A: Physical*, 52(1), 8-11. doi:10.1016/0924-4247(96)80118-X
- Xiong, H., & Wang, L. (2016). Piezoelectric energy harvester for public roadway: On-site installation and evaluation. *Applied Energy*, 174, 101-107.
- Xu, T., Jiang, X., & Su, J. (2011). A piezoelectric multilayer-stacked hybrid actuation/transduction system. *Applied Physics Letters*, 98(24), 243503.
- Yang, Y., & Tang, L. (2009). Equivalent circuit modeling of piezoelectric energy harvesters. *Journal of Intelligent Material Systems and Structures*, 20(18), 2223-2235.
- Yang, Z., Erturk, A., & Zu, J. (2017). On the efficiency of piezoelectric energy harvesters. *Extreme Mechanics Letters*, 15, 26-37.

- Yang, Z., Zhu, Y., & Zu, J. (2015). Theoretical and experimental investigation of a nonlinear compressive-mode energy harvester with high power output under weak excitations. *Smart Materials and Structures*, 24(2), 025028.
- Yang, Z., & Zu, J. (2014). High-efficiency compressive-mode energy harvester enhanced by a multi-stage force amplification mechanism. *Energy Conversion and Management*, 88, 829-833.
- Zhang, X., Zhang, Z., Pan, H., Salman, W., Yuan, Y., & Liu, Y. (2016). A portable high-efficiency electromagnetic energy harvesting system using supercapacitors for renewable energy applications in railroads. *Energy Conversion and Management*, 118, 287-294. doi:<https://doi.org/10.1016/j.enconman.2016.04.012>
- Zhou, S., Chen, W., Malakooti, M. H., Cao, J., & Inman, D. J. (2017). Design and modeling of a flexible longitudinal zigzag structure for enhanced vibration energy harvesting. *Journal of Intelligent Material Systems and Structures*, 28(3), 367-380.
- Zhou, Z., Wang, X., Zhang, X., Chen, G., Zuo, J., & Pullen, S. (2015). Effectiveness of pavement-solar energy system – an experimental study. *Applied Energy*, 138, 1-10. doi:10.1016/j.apenergy.2014.10.045

## BIOGRAPHICAL SKETCH

Adriana Rosas earned a B.S Civil Engineering degree from the University of Texas Rio Grande Valley in 2019 followed by a M.S in Civil Engineering in 2022. Adriana may be reached at [Rosas.adriana13@gmail.com](mailto:Rosas.adriana13@gmail.com).